Energy 265 (2023) 126186

Contents lists available at ScienceDirect

Energy

journal homepage: www.elsevier.com/locate/energy

ORC fluids selection for a bottoming binary geothermal power plant integrated with a CSP plant

T.E. Boukelia [a,b,*], O. Arslan [c], S. Djimli [d], Y. Kabar [b]

[a] Mechanical Engineering Department, Jijel University, Jijel, Algeria
[b] Mechanical and Advanced Materials Laboratory, Polytechnic School of Constantine, Constantine, Algeria
[c] Mechanical Engineering Department, Engineering Faculty, Bilecik Seyh Edebali University, Bilecik, Turkey
[d] Laboratory of Applied Energetics and Materials, Mechanical Engineering Department, Jijel University, Jijel, Algeria

ARTICLE INFO

Keywords:
Bottoming binary geothermal
Combined
Fluid selection
Performance
Topping solar plant

ABSTRACT

Hybridization of geothermal power plants with concentrating solar power systems is an attractive solution to enhance the dispatch capacity of thermal power plants. Hence, the design and thermo-economic analyses of a combined solar-geothermal power plant with different organic fluids have been investigated. This configuration generates electricity at two temperature levels; high one at a topping parabolic trough solar power plant, and low one at a bottoming binary geothermal plant. The topping solar plant is equipped with energy storage and fuel backup systems simultaneously to maximize the generated power. Furthermore, the bottoming geothermal plant has been analyzed with nine different organic fluids.

The obtained results show that power generation of this configuration has been raised by more than 19.36% at nominal conditions compared to the reference stand-alone solar plant. Moreover, organic fluids with wet behavior show better performances than those with dry one. In this regard, ammonia, R32, R290, and R143a are more efficient than the others, where annual net outputs of 22.20, 20.02, 19.25, and 18.67 GWh_e have been produced, respectively. Furthermore, the combined plant with ammonia as the working fluid in the bottoming installation has the lowest levelized cost of electricity with a value of 10.42 ¢/kWh.

1. Introduction

The energy sector is experiencing a massive and accelerating increase in global demand for clean energy due to economic trends, population growth, and global warming. On the other hand, conversion systems based on renewable energy resources can play an essential role in generating clean and stable power. In this regard, concentrating solar power (CSP) systems seem to be one of the most mature technologies available in the market to achieve this task. These systems generally work with high temperatures that can reach 1000 °C [1]. Moreover, binary geothermal power plants (BGPP) are another solution to generate clean energy based on low-temperature geothermal sources. However, these systems suffer from low dispatchability and high investment costs.

Since there is a vast geographical coincidence of geothermal resources with abundant sunshine areas from a side, and high possibility of technical integration of the BGPP as a bottoming system to recuperate the wasted heat from the high temperature topping CSP plant on the other side, hybridization of these two technologies is an excellent alternative to enhance the dispatchability of large-scale power plants, and decrease their investment cost. Thus, many papers have been published to assess the technical and economical potentials of these hybrid plants [2–10]. On the same wave, another simulation work has been presented by Bonyadi et al. [11]. They proposed a new combined solar-geothermal plant to generate power. In this regard, an existing bottoming BGPP is integrated with a topping steam Rankine cycle to generate power at two levels; low and high temperatures. While Keshvarparast et al. [12] analyzed thermodynamic performances of a hybrid parabolic trough-geothermal binary plant. Besides, they presented a parametric analysis of different working factors such as ambient temperature, fluid type, and mass flow rates on the thermodynamic performances in typical days of cold and hot months. Moreover, Jiang and his team [13] presented an enhanced geothermal system coupled with a supercritical solar power plant to enhance its capacity factor. The working fluid in both systems is CO_2. Also, a comparison was made between the performances of the new hybrid system alongside stand-alone layouts. A multi-objective optimization was performed by Nazari et al. [14] to enhance the exergo-economic performances of a

* Corresponding author. Mechanical Engineering Department, Jijel University, Jijel, Algeria.
E-mail address: taqy25000@hotmail.com (T.E. Boukelia).

https://doi.org/10.1016/j.energy.2022.126186
Received 10 February 2022; Received in revised form 11 November 2022; Accepted 23 November 2022
Available online 2 December 2022

Nomenclature

γ_{col}	Collector orientation with the azimuth angle [°]
γ_s	Azimuth angle [°]
Δ_{tes}	Total storage hours [hour]
ΔT_{LMTD}	Logarithmic mean temperature difference [°C]
η_{BBGPP}	Overall energy efficiency of the BBGPP [−]
$\eta_{ene,SF}$	Energy efficiency of the solar field [−]
$\eta_{endLoss}$	Spillage end losses [−]
$\eta_{gen,col}$	Collector general errors [−]
$\eta_{geo,col}$	Collector geometry imperfection [−]
$\eta_{isen,OP}$	Isentropic efficiency of the organic pump [−]
$\eta_{isen,OT}$	Isentropic efficiency of the organic turbine [−]
$\eta_{off,OP}$	Off-design efficiency of the organic pump [−]
$\eta_{off,OT}$	Off-design efficiency of the organic turbine [−]
η_{opt}	Optical efficiency of the solar field [−]
$\eta_{PB\ des}$	Power cycle efficiency at the design point [−]
η_{Plant}	Overall energy efficiency of the whole hybrid plant [−]
η_{shad}	Shading effect losses [−]
η_{soil}	Collector soiling [−]
η_{TPTPP}	Overall energy efficiency of the topping parabolic trough power plant [−]
$\eta_{track,col}$	Collector tracking error [−]
θ	Incidence angle [°]
θ_c	Elevation angle [°]
θ_{col}	Tilt angle of the collector [°]
ρ_m	Mirror reflectance [−]
ω	Aperture width of the collector [m]
ω_{col}	Collector tracking angle [°]
A_{cond}	Surface area of the condenser in the BBGPP [m^2]
A_{evap}	Surface area of the evaporator in the BBGPP [m^2]
A_{SF}	Total area of the solar field [m^2]
C_{inv}	Total investment costs [M$]
$C_{O\&M}$	Operation and maintenance costs [M$]
CF	Capacity factor [%]
f_{backup}	Fossil fill fraction [−]
h	Enthalpy at each point of the installation [kJ/kg]
$h_{in\ turbine}$	Enthalpy at the inlet of the steam turbine [kJ/kg]
h_{SFi}	Enthalpy at the inlet of the solar field [kJ/kg]
h_{SFo}	Enthalpy at the outlet of the solar field [kJ/kg]
I_{bn}	Hourly direct normal irradiance [kW/m^2]
k_d	Annual discount rate [%]
IAM	Incidence angle modifier [−]
L_{col}	Length of the parabolic trough collector [m]
$L_{f,ave}$	Average focal length of the parabolic trough collector [m]
$L_{spacing}$	Distance between collector rows [m]
LCOE	Levelized cost of electricity [¢$/kWh]
$\dot{m}_{cw}$	Mass flow rate of the cooling water of the BBGPP [kg/s]
$\dot{m}_{geo}$	Mass flow rate of the geothermal water [kg/s]
$\dot{m}_{HTF}$	Mass flow rate of the heat transfer fluid in the TPTPP [kg/s]
$\dot{m}_{of}$	Mass flow rate of the organic fluid [kg/s]
N	Depreciation operation time of the system [yrs]
ND	Number of the days in a year [−]
N_{sca}	Number of collector assemblies per loop [−]
$\dot{Q}_{evap}$	Energy transferred through the evaporator of the BBGPP [kW]
$\dot{Q}_{FBS}$	Thermal energy must be supplied by the FBS [kW]
$\dot{Q}_{geo}$	Energy flow from the geothermal source [kW]
$\dot{Q}_{hl}$	Total heat loss from the receiver of solar collector [kW]
$\dot{Q}_{HTF}$	Energy absorbed by the heat transfer fluid [kW]
$\dot{Q}_{inc}$	Total energy incident on the solar field [kW]
$\dot{Q}_{rec,BBGPP}$	Total energy recuperated by the BBGPP [kW]
$\dot{Q}_{rej,TPTPP}$	Total energy rejected by the TPTPP [kW]
$PG_{BBGPP,net}$	Net power generation by the BBGPP [kWh]
$PG_{Plant,net}$	Net power generation by the whole combined plant [kWh]
$PG_{TPTPP,net}$	Net power generation by the TPTPP [kWh]
R_{cond}	Heat transfer resistance by conduction through the tube wall [K/m]
R_{conv}	Heat transfer resistance by convection from the inner tube wall to HTF [K/m]
r_H	Ratio of enthalpy drop in the organic turbine between the off-design and design conditions [−]
$r_{H,OT}$	Deviation coefficient due to enthalpy drop [−]
r_V	Ratio of volumetric flow rate drop in the organic turbine between the off-design and design conditions [−]
$r_{V,OT}$	Deviation coefficient due to volumetric flow rate drop [−]
T_{amb}	Ambient temperature [K]
T_{sky}	Sky temperature [K]
U_{evap}	Overall heat transfer coefficient of the evaporator [kW/m^2 °C]
U_{evap}	Overall heat transfer coefficient of the condenser [kW/m^2 °C]
$\dot{V}_{of}$	Volumetric flow rate of the organic fluid [m^3/s]
$\dot{W}_{OP}$	Power consumed by the organic pump [kW]
$\dot{W}_{OT}$	Power produced by the organic turbine [kW]

Abbreviation

BBGPP	Bottoming binary geothermal power plant
BGPP	Binary geothermal power plant
CON	Condenser
CP	Condenser pump
CSP	Concentrating solar power
DEA	Deaerator
DNI	Direct normal irradiance
DP	Deaerator pump
EVAP	Evaporator
FBS	Fuel backup system
FWH	Closed feedwater heater
GEN	Generator
HF	Heliostat field
HPT	High-pressure turbine
HTF	Heat transfer fluid
LPT	Low-pressure turbine
NREL	National Renewable Energy Laboratory
OF	Organic fluid
OP	Organic pump
ORBPB	Organic Rankine bottoming power block
ORC	Organic Rankine cycle
OT	Organic turbine
PB	Power block
PTC	Parabolic trough collector
PTPP	Parabolic trough power plant
PH	Preheater
RH	Reheater
RTPB	Rankine topping power block
SAM	System Advisor Model
SAPTPP	Stand-alone parabolic trough power plant
SF	Solar field
SG	Steam generator
SP	Superheater
SR	Solar receiver
T	Tower
TES	Thermal energy storage
TPB	Topping power block
TPTPP	Topping parabolic trough power plant

combined steam-organic Rankine plant that can recuperate the wasted heat of a topping gas turbine. Thus, three organic fluids were analyzed, and subcritical and transcritical cycles were selected for the steam and the organic Rankine cycles respectively. Motivated by consistency in high ambient temperatures and high solar radiation levels, Heberle et al. [15], explored the performances of incorporating an air-cooled geothermal binary power plant and a solar thermal plant to retrofit the yield of these systems. The techno-economic criteria have been presented, and climatic conditions of Turkey were considered in the simulations. McTigue et al. [16] proposed to integrate a double-flash geothermal plant and thermal energy storage to improve the potential of a solar thermal power plant based on linear Fresnel reflector technology using synthetic oil as the primary working fluid in the solar field. Furthermore, optimal design and economic feasibility of the simulated plant were also considered. Another thermodynamic analysis of integrating a solar field to an ORC binary geothermal power plant to produce power has been introduced by Acar and Arslan [17]. R600a is chosen as the heat transfer fluid in the geothermal block, while Therminol oil transfers the heat in the solar field. Moreover, Li et al. [18] proposed to use a solar field working with a high temperature as a heat source to raise the dispatchability of a geothermal plant based on a two-stage serial organic Rankine cycle. The proposed system was simulated and optimized. The performances of a hybrid geothermal-solar power plant have been modeled and enhanced by Bassetti et al. [19]. In their layout, air-cooled ORC and thermal energy storage systems are used. Many more papers have been presented in the literature on modeling and simulation of hybrid CSP-geothermal power plants [20–23]. However, and according to our knowledge, it seems that most published works are taking one of the two heat sources, either solar or geothermal, as a supplementary heat source to raise the generated power of the other block.

Moving through literature based on the fluid selection in the organic Rankine cycles, many published papers have been reported to analyze the performances of using different organic fluids in ORC for various applications such as waste heat recovery, cooling, and heating, as well as power generation. Wang et al. [24] emphasized that fluid selection in designing ORC is a crucial factor. They performed a new approach based on both economic and environmental dimensions to optimize this procedure, and a heat source with a temperature that varies from 90 to 230 °C has been considered. As a result, they matched between every heat source temperature range and corresponding fluids. Zhang et al. [25] established a multi-parameter optimization model of an ORC for medium-to-high temperature wasted heat recovery. In this regard, 42 pure organic fluids have been screened according to their environmental performances, and the relationship between source temperature, fluid properties, system parameters, and performance has been described. Furthermore, Sachdeva and Singh [26] presented the effect of using three different organic fluids in a bottoming ORC of a triple combined cycle powered by solar tower technology. The combined plant is divided into three power blocks; a topping Brayton cycle to convert received heat from the high-temperature solar field to power, steam and organic Rankine cycles as bottoming power blocks for waste heat recovery. Cataldo and his colleagues [27] proposed a methodology based on a genetic algorithm for fluid selection of an ORC for low-temperature waste heat recovery. Consequently, three inputs are taken as decision variables, including working fluid, evaporation and condensation temperatures, while two objective functions are aimed; defect of cycle efficiency and heat exchange area per unit of generating power. While Tchanche and his team [28] compared the performances of using 20 different organic fluids in a low-temperature solar organic Rankine power plant. These performances were presented in terms of efficiencies, volume flow rates, pressure ratios, toxicity, flammability, ODP, and GWP. Drescher and Bruggemann [29] explored the selection procedure in a small-scale biomass power plant for cogeneration (power and heat generation). Hærvig et al. [30] screened 26 commonly used organic fluids based on a systematic approach. This approach considered the genetic algorithm to optimize the working conditions of an ORC and the mixture composition of the fluids, and a heat source with a temperature range of 50–280 °C is presented. A parametric optimization using a multi-objective optimization approach has been performed by Wang et al. [31] to optimize and compare 13 different working fluids in an ORC for low-temperature waste heat recovery. The exchanger area per power output unit and the heat recovery efficiency have been selected as the objective functions, while evaporation and condensation pressures, working fluid, and mass flow rates are considered as the inputs. Many more works have been reported in the literature based on the fluid selection in organic Rankine cycles [32–43]. However, to sum up, it can be concluded from the literature that the fluid selection approach is not reported for hybrid solar-geothermal plants with such a layout. Besides, this study will be the first attempt that explores fluid selection based on thermo-economic criteria for these hybrid plants for large-scale power generation at two temperature levels; high one (for TPTPP) and low one (for BBGPP).

Thus, this paper presents the design and annual techno-economic performance assessment of a combined solar-geothermal power plant with different organic fluids to choose the best fluid to be employed. This plant is based on a combined configuration with a bottoming binary geothermal cycle that recuperates the wasted heat from a topping solar thermal power layout to boost the dispatch capacity of the whole plant and enhance its thermo-economic performances. This paper can give new insights on enhancing the dispatch capacity and raising the thermo-economic performances of hybrid thermal power plants, including those based on renewable energies, either by hybridization or waste heat recovery. These techniques can be explored in other technologies besides solar and geothermal, such as coal, natural gas, and biomass.

2. Data and methodology

The main aim of this work is to simulate the thermo-economic performances of using different organic fluids as candidates for a bottoming binary geothermal power plant (BBGPP). This BBGPP is integrated with a topping parabolic trough power plant (TPTPP), where the geothermal source with low-enthalpy will gain additional heat from the TPTPP to improve the generated power of the bottoming cycle. The design of the solar block is based on an existing PTPP, which is similar to the combined Archimede layout [44,45], and incorporated with two auxiliaries; thermal energy storage (TES) and fuel backup system (FBS). The primary working fluid both in the solar field and the storage system is molten salt. On the other hand, the BBGPP is designed to be the bottoming side of the studied combined plant, which is similar to an existing AFJET power plant [46]. Nine organic fluids are selected to choose the best candidates as the primary fluid in the BBGPP. For this aim, a defined methodology is selected and presented in Fig. 1. Furthermore, different assumptions, inputs, and mathematical modeling of the studied plant are presented in the following sub-sections.

2.1. Site selection

In the present work, El Oued (South-East of Algeria) has been chosen for the simulations, it is characterized by its relatively high solar radiation and geothermal sources of low-temperature range. Its environmental and ambient conditions are summarized in Table 1 [47,48].

2.2. Studied plant

In the investigated combined solar-geothermal plant, the solar field (SF) of the TPTPP is made up of many sun-tracking East-West [49] parabolic trough collectors with a total area of more than 31,860 m^2. The solar radiation is concentrated on solar receivers (SR) by parabolic trough collectors (PTC). Consequently, the working fluid (molten salt) circulating inside the receivers is heated to transfer the gained heat to the steam Rankine cycle to generate superheated steam through a series

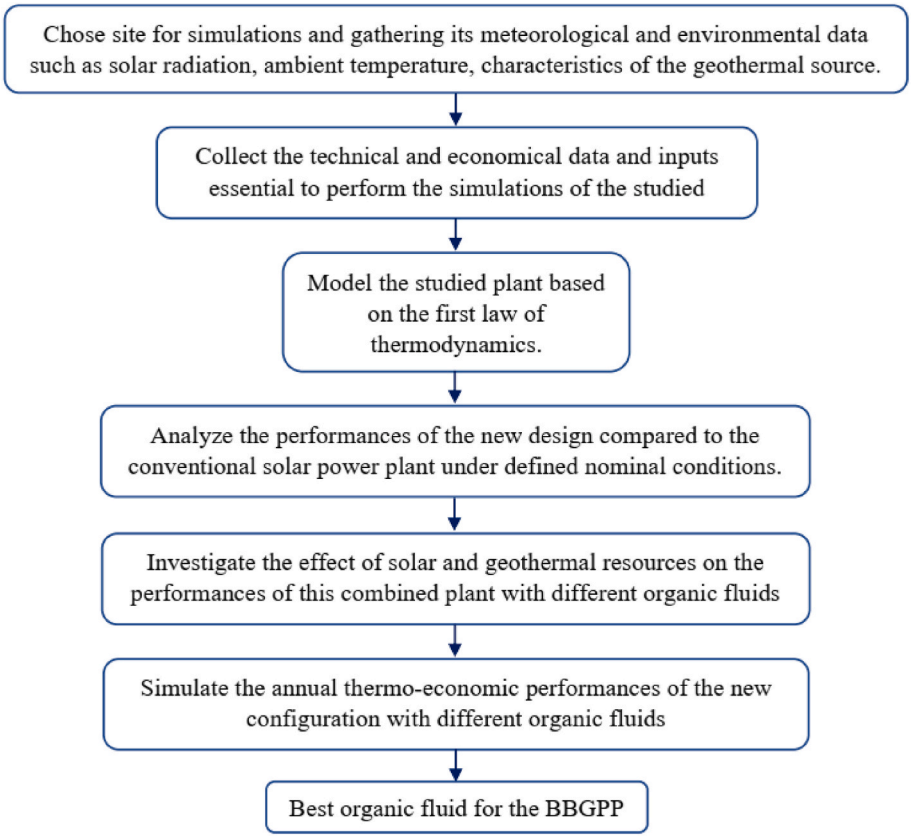

Fig. 1. Main steps of the proposed methodology to perform the study.

Table 1
Properties of solar and geothermal sources of the chosen location.

Parameter	Value
Annual DNI [kWh/m^2]	2035
Annual mean ambient temperature [°C]	21.8
Temperature at production well [°C]	65
Mass flow rate of the geothermal fluid [kg/s]	100

of heat exchangers (preheater, steam generator, and superheater). Then this superheated steam, which is used to produce electrical power, in turn, will be expended in different stages of high (HPT) and low (LPT) pressure turbines. Furthermore, two auxiliaries are equipped within the installation; TES and FBS to provide additional thermal energy if the required state at the HPT inlet is not reached, hence, increase the capacity factor of the TPTPP. On the other hand, a BBGPP similar to the existing AFJET plant [46] is presented as a bottoming installation. In this configuration, the hot water from the geothermal production well is pumped through the condenser (CON1) to get the rejected thermal energy of the TPTPP and ensure its cooling process. Then, this hot geothermal water exchanges its heat with an organic fluid through an evaporator. This organic fluid with vapor phase is used to operate the organic turbine (OT) to generate electricity at a low temperature. Then, this steam leaving the OT is condensed inside the condenser (CON2), and the process starts over for a new cycle.

In the present paper, at the design point, a gross capacity of 5 MW is assumed for the TPTPP. The investigated hybrid plant is presented in Fig. 2, and its main technical inputs and data, including those of the TPTPP and the BBGPP are presented in Tables 2 and 3. Furthermore, the main aim of this work is to explore different organic fluids to choose the best fluids to be adopted in the bottoming plant, which give the highest performances of the new plant. Thus, different organic fluids (OF) will be investigated.

It should be pointed out that to ensure the effectiveness of the cooling process in the topping steam power block, the temperature of the hot water from the geothermal production well (which is the cooling fluid in this case) should be lower than that of the steam at the inlet of the condenser. Thus, the high value of the leaving pressure presented in Table 2 is an obligation to ensure the cooling process, although it increases the wasted heat; hence, it decreases the generated power of the TPTPP. Consequently, for the given geothermal source temperature of 65 °C in this work, a high value for the condensing pressure in the TPTPP of 50 kPa should be considered [53].

CON: Condenser, CP: Condenser Pump, CT: Cooling Tower, DEA: Deaerator, DP: Deaerator Pump, ET: Expansion tank, EVAP: Evaporator, FWH: Feed Water Heater, GEN: Generator, HPT: High Pressure Turbine, LPT: Low Pressure Turbine, OT: Organic Turbine, OP: Organic Pump, PH: Pre-Heater, RH: Re-Heater, SG: Steam Generator, TSS: Thermal Storage System, FBS: Fuel Backup System, SF: Solar field.

2.3. Energy model

2.3.1. TPTPP

As mentioned in section 2, a design similar to the Archimede power plant is investigated in the TPTPP. In this layout, molten nitrate salt (60% $NaNO_3$+ 40% KNO_3) with a working temperature range of 290–550 °C is chosen as the heat transfer fluid (HTF) both in the SF and the TES. In the modeling process, the empirical equations for the thermophysical properties of the employed fluids in the topping plant, including molten salt, and water/steam, were considered [54,55]. The energy model of the TPTPP is summarized as a segregated formulation of each system, including solar field, auxiliaries, and power block in the following subsections.

2.3.1.1. Solar field. The energy efficiency of the solar field extends to estimate both optical and thermal losses, which can be defined by the

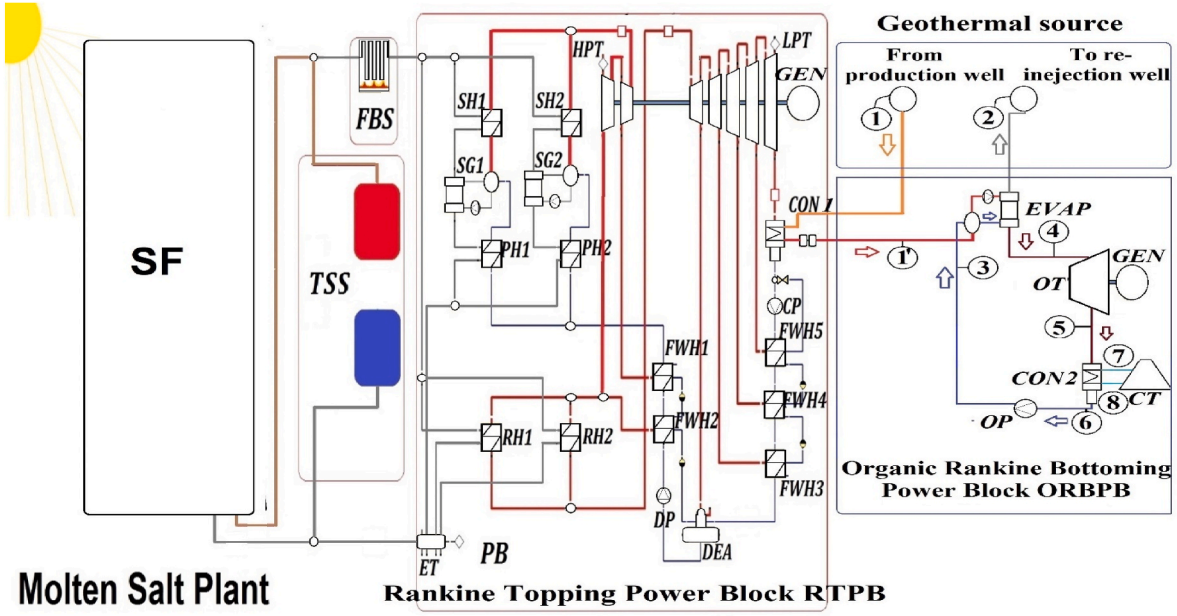

CON: Condenser, CP: Condenser Pump, CT: Cooling Tower, DEA: Deaerator, DP: Deaerator Pump, ET: Expansion tank, EVAP: Evaporator, FWH: Feed Water Heater, GEN: Generator, HPT: High Pressure Turbine, LPT: Low Pressure Turbine, OT: Organic Turbine, OP: Organic Pump, PH: Pre-Heater, RH: Re-Heater, SG: Steam Generator, TSS: Thermal Storage System, FBS: Fuel Backup System, SF: Solar field.

Fig. 2. Studied hybrid solar-geothermal thermal power plant.

Table 2
The main inputs of the TPTPP [23,44,45,50].

System	Parameter	Value
Solar field (SF)	Working fluid [−]	60% $NaNO_3$+ 40% KNO_3
	Inlet working temperature [°C]	290
	Outlet working temperature [°C]	550
	Total solar field surface area [m^2]	31,810
	Collector orientation [−]	N–S
	Row spacing [m]	15
	Collector design [−]	Solargenix SGX-1
	Receiver design [−]	Schott PTR70
	Aperture width [m]	5
	Length of collector assembly [m]	100
	Focal length [m]	1.8
	Number of modules per assembly	12
	Absorber tube inner/outer diameter [m]	0.066/0.070
	Glass envelope inner diameter [m]	0.115/0.120
Topping power block (TPB)	Working fluid [−]	Steam/Water
	Design turbine gross output [MWe]	4.8
	HPT isentropic efficiency [%]	0.85
	LPT isentropic efficiency [%]	0.88
	Leaving pressure [kPa]	50
	Feedwater pump isentropic efficiency [%]	0.80
	Condensate pump isentropic efficiency [%]	0.80
	Generator efficiency [%]	0.97
Fuel backup system (FBS)	Fossil fuel fill fraction [−]	0.27
	FBS boiler efficiency [%]	90
Thermal energy storage (TES) system	Storage type [−]	Two tank molten salt
	Full load hours [hours]	7.5

Table 3
The main inputs of the BBGPP [17–20,51,52].

System	Parameter	Value
Geothermal source	Temperature at production well [°C]	65
	Temperature at re-injection well [°C]	35
	Mass flow rate of the geothermal fluid [kg/s]	81
	Pressure of the geothermal source [kPa]	220
Organic Rankine bottoming power block (ORBPB)	Turbine isentropic efficiency [%]	0.85
	Pump isentropic efficiency [%]	0.80
	Generator efficiency [%]	0.97
	Overall heat transfer coefficient of the evaporator [kW/m^2 °C]	0.90
	Overall heat transfer coefficient of the condenser [kW/m^2 °C]	1.00

ratio of the gained heat by the HTF to the total incident solar radiation on the total surface area of the SF, or can be expressed mathematically by the following equation:

$$\eta_{ene,SF} = \frac{\dot{Q}_{HTF}}{\dot{Q}_{inc}} \quad (1)$$

Where $\dot{Q}_{inc}$ is the solar flux incident on the SF, and formulated by:

$$\dot{Q}_{inc} = I_{bn} A_{SF} \eta_{opt} \quad (2)$$

In this equation, the optical efficiency can be defined mathematically as:

$$\eta_{opt} = \eta_{endLoss} \times \eta_{shad} \times \eta_{IAM} \times \eta_{geo,col} \times \eta_{track,col} \times \rho_m \times \eta_{soil} \times \eta_{gen,col} \quad (3)$$

Where $\eta_{endLoss}, \eta_{shad}, \eta_{IAM}, \eta_{geo,col}, \eta_{track,col}, \rho_m, \eta_{soil}, \eta_{gen,col}$ are defined in the nomenclature section. These terms can be estimated by equations (4)–(6) [56,57]:

$$\eta_{endLoss} = 1 - L_{f,ave} \tan\theta - \left(\frac{N_{sca}}{2} - 1\right) \frac{2\left(L_{f,ave} \tan\theta - L_{Spacing}\right)}{N_{sca} - L_{col}} \quad (4)$$

$$\eta_{shad} = |\sin(90^\circ - \omega_{col})| \frac{L_{Spacing}}{\omega} \quad (5)$$

$$IAM = 1 + 0.000884 \bullet \frac{\theta}{\cos\theta} - 0.00005369 \bullet \frac{\theta^2}{\cos\theta} \quad (6)$$

Where ω_{col}, N_{sca} $L_{f,ave}$, $L_{spacing}$, ω, and L_{col} represent the collector tracking angle, the number of collector assemblies per loop, the average focal length, the distance between collector rows, the aperture width and length of the collector, respectively. Furthermore, the incidence angle can be estimated as:

$$\theta = \cos^{-1}\sqrt{1 - [\cos(\theta_c - \theta_{col}) - \cos(\theta_{col})\cos(\theta_c)(1 - \cos(\gamma_s - \gamma_{col}))]^2} \quad (7)$$

On the other hand, the useful heat from the SF can be calculated as:

$$\dot{Q}_{HTF} = \dot{Q}_{inc} - \dot{Q}_{hl} = \dot{m}_{HTF} \times (h_{SFo} - h_{SFi}) \quad (8)$$

where the heat losses in each solar receiver of the PTC considering the three heat transfer phenomena (Fig. 3) are estimated by Refs. [56,57]:

$$\dot{Q}_{hl} = \frac{(T_3 - T_{amb})R_{5,7\ rad} + (T_3 - T_6)R_{5,6\ conv} - \dot{q}_{abs,env}\Omega_R}{R_{3,4\ tot}R_{5,7\ rad} + R_{3,4\ tot}R_{5,6\ conv} + \Omega_R} \quad (9)$$

With $T_6 = T_{sky}$, and $T_7 = T_{amb}$, and:

$$\Omega_R = R_{5,6\ conv}R_{5,7\ rad} + R_{4,5\ cond}R_{5,7\ rad} + R_{4,5\ cond}R_{5,6\ conv} \quad (10)$$

2.3.1.2. Auxiliaries systems (TES and FBS). Generally, CSP plants can be equipped with thermal storage and fuel backup systems to raise the capacity factor of such type of thermal power plants. Consequently, the studied plant encompasses the two auxiliaries simultaneously to raise its dispatch capacity. In this regard, the two most important parameters to consider in the two systems are [56,59]:

$$E_{tes} = \frac{w_{des}\Delta_{tes}}{\eta_{PB\ des}} \quad (11)$$

$$f_{backup} = \frac{\dot{Q}_{FBS}}{\dot{Q}_{tot}} \quad (12)$$

Where $\dot{Q}_{FBS}$ is the thermal energy to be supplied by the FBS, and it is given by eq. (13):

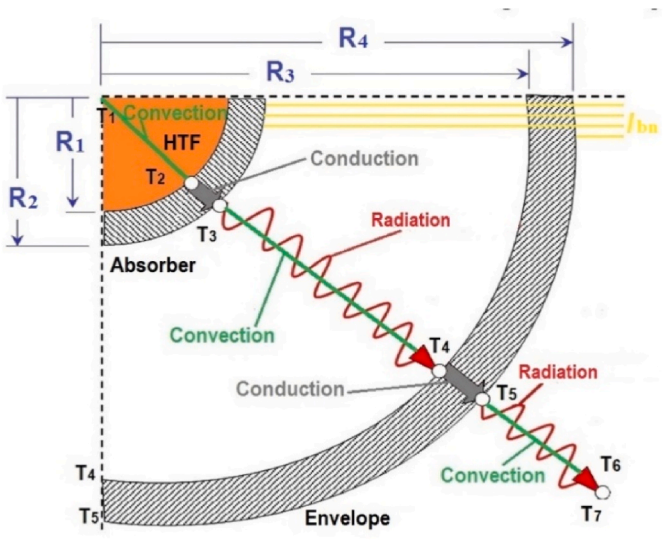

Fig. 3. Phenomena of heat transfer in the HCE [58].

$$\dot{Q}_{FBS} = \dot{m}_{HTF}(h_{in\ \ turbine} - h_{SFO}) \quad (13)$$

Where E_{tss} formulates the potential number of hours that the storage system can supply heat to the topping power block, while f_{backup} defines the fossil fill fraction of the fuel backup system. The values of these two parameters are given in Table 2.

2.3.1.3. Topping power block (TPB). For the topping power block (TPB), its energy model is simulated within SAM based on regression equations in a normalized form to consider the off-design simulations, and can be presented as [60]:

$$y = f(\dot{m}_{HTF\ PB}, T_{HTF}, T_{amb}) \quad (14)$$

Therefore, the energy efficiency of the topping parabolic trough power plant is given by:

$$\eta_{TPTPP} = \frac{PG_{TPTPP,net}}{\dot{Q}_{inc}} \quad (15)$$

The energy models, including those of pipe losses and system parasitic of the whole TPTPP and its subsystems, are well presented in details in Refs. [56–60].

2.3.2. BBGPP

2.3.2.1. Design modeling. For the energy modeling of the BBGPP, a simple organic Rankine cycle (ORC) structure under sub-critical conditions is defined. In this regard, nine different organic fluids have been chosen, and their thermo-physical properties are considered and discussed in section 2.3.3. On the other hand, as presented in Table 3, the working turbine, pump, and electric generator efficiencies in the ORC are taken 0.85, 0.80, and 0.97, respectively at design condition. Besides, a pinch temperature difference for the evaporator and condenser is assumed to be 15 °C, and a minimum superheat degree of 5 °C for the considered fluids to avoid liquid droplets [17–20,25,51,52]. Mass and energy balances were applied to every system component. Thus, the wasted heat recovered by the geothermal water of the production well from the TPTPP's condenser is estimated by:

$$\dot{Q}_{rec,BBGPP} = \dot{m}_{geo}(h_{1'} - h_1) \quad (16)$$

Where h_1 and $h_{1'}$ are the enthalpies of the geothermal water at the inlet and outlet of the TPTPP's condenser.

The gained heat by the organic fluid through the evaporator from the geothermal water leaving the CON1 is presented by:

$$\dot{Q}_{evap} = \dot{m}_{geo}(h_{1'} - h_2) = \dot{m}_{of}(h_4 - h_3) = U_{evap}A_{evap}\Delta T_{LMTD} \quad (17)$$

While the produced electricity by the organic turbine, the consumed power by the pump, and the net generated power by the BBGPP, are given by equations (18)–(20), respectively:

$$\dot{W}_{OT} = \dot{m}_{of}(h_4 - h_3) \times \eta_{isen,OT} \times \eta_{Gen} \quad (18)$$

$$\dot{W}_{OP} = \dot{m}_{of}(h_3 - h_6) \times \eta_{isen,OP} \quad (19)$$

$$PG_{BBGPP,net} = \dot{W}_{OT} - \dot{W}_{OP} \quad (20)$$

The terms h_3, h_4 and h_6 present the enthalpies at the outlet of the pump, of the evaporator, and of the condenser respectively. While $\eta_{isen,OT}$, $\eta_{isen,OP}$, and η_{Gen} refer to the efficiencies of the turbine, the pump, and the generator of the BBGPP. On the other hand, $U_{evap}A_{evap}$ defines the product of the overall heat coefficient and surface area of the evaporator.

Furthermore, the rejected thermal energy to condense the organic fluid is calculated by:

$$\dot{Q}_{cond} = \dot{m}_{of}(h_{1'} - h_2) = \dot{m}_{cw}(h_8 - h_7) = U_{cond}A_{cond}\Delta T_{LMTD} \quad (21)$$

$U_{cond}A_{cond}$ presents the product of the overall heat coefficient and surface area of the condenser, while h_7 and h_8 are the enthalpies of the cooling water at the inlet and outlet of the BBGPP's condenser.

In order to estimate the heat transfer area of the evaporator and the condenser in equations (17) and (21), the logarithmic mean temperature difference (LMTD) method is used:

$$\Delta T_{LMTD} = \frac{\Delta T_{max} - \Delta T_{min}}{ln\left(\frac{\Delta T_{max}}{\Delta T_{min}}\right)} \tag{22}$$

Where ΔT_{max} and ΔT_{min} represent the maximal and the minimal temperature differences of the two heat exchangers, respectively.

Thus, the energy efficiency of the BBGPP can be given by:

$$\eta_{BBGPP} = \frac{PG_{BBGPP,net}}{\dot{Q}_{geo}} = \frac{PG_{BBGPP,net}}{\dot{m}_{geo}(h_{1'} - h_2)} \tag{23}$$

Therefore, the energy efficiency of the whole hybrid installation (CSP-geothermal plant), it can be calculated by:

$$\eta_{Plant} = \frac{PG_{Plant,net}}{\dot{Q}_{inc} + \dot{Q}_{geo}} = \frac{PG_{TPTPP,net} + PG_{BBGPP,net}}{\dot{Q}_{inc} + \dot{Q}_{geo}} \tag{24}$$

At the end, the capacity factor, which expresses the distribution of generated power of the simulated plant during the whole year of operation, it is introduced by the following equation:

$$CF = \frac{PG_{Plant,net}}{ND.\left(24\,\frac{hr}{day}\right).5\ MW} \tag{25}$$

2.3.2.2. Off-design modeling. To consider the fluctuating ambient temperature and received heat flux from the topping solar installation, off-design modeling should be considered to avoid miscalculations of the BBGPP performances. Thus, the turbine and pump efficiencies, global heat transfer coefficients are varied during the simulations. The turbine isentropic efficiency is calculated as [61]:

$$\eta_{off,OT} = \eta_{isen,OT} \times r_{H,OT} \times r_{V,OT} \tag{26}$$

Where $r_{H,OT}$ and $r_{V,OT}$ are deviations coefficients due to enthalpy and volumetric flow rate drops and are given by Ref. [61]:

$$r_{H,OT} = (((1.398r_H - 5.425) \times r_H + 6.274) \times r_H - 1.866) \times r_H \tag{27}$$

$$r_{V,OT} = (((-0.21r_V + 1.117) \times r_V - 2.533) \times r_V + 2.588) \times r_V \tag{28}$$

r_H and r_V are the ratios of drops in the enthalpy and in the volumetric flow rate between the off-design conditions and those at nominal (design) state:

$$r_H = \sqrt{(h_4 - h_5)\Big/(h_4 - h_5)^d} \tag{29}$$

$$r_V = \sqrt{\dot{V}_{of}/\dot{V}_{of}^{\ d}} \tag{30}$$

The index d here refers to the design state, while $\dot{V}_{of}$ is the volumetric flow rate of the organic fluid.

Moving to the efficiency of the organic pump at off-design conditions, it can be calculated by the following correlation [62]:

$$\eta_{off,OP} = 2\eta_{isen,OT} \times \frac{\dot{V}_{of}}{\dot{V}_{of}^{\ d}} - \eta_{isen,OT} \times \left(\frac{\dot{V}_{of}}{\dot{V}_{of}^{\ d}}\right)^2 \tag{31}$$

For the heat exchangers (the evaporator and the condenser), their overall heat transfer coefficients at off-design conditions are calculated by Ref. [5]:

$$U_{off} = U^d\left(\frac{\dot{m}_{of}}{\dot{m}_{of}^{\ d}}\right)^m \tag{32}$$

where m is taken 0.8 and 0.7 for internal and external flow respectively.

2.3.3. Organic fluid selection

In energy conversion systems based on organic fluids (OF), the thermophysical properties of such fluids affect the design and the control strategy of these systems, and determine their techno-economic performances. On the other side, and to compare different well-known fluids based on their performances, cycle yields are always estimated based on the thermodynamic properties of these OFs [25]. Thus, in the present study, the thermos-physical properties of 9 pure working fluids were illustrated out from the database REFPROP 9.0 developed by NIST [63]. These fluids have been selected and grouped according to their critical temperature into three levels; (1) T_{cri} <100 °C, (2) 100 < T_{cri} <150 °C, and (3) 150 < T_{cri} < 300 °C, and for each level, three different fluids have been chosen. These fluids are summarized along with their properties in Table 4.

2.4. Economic model

In the present work, the economic analysis of the investigated combined CSP-geothermal power plant with the nine layouts in the BBGPP was carried out based on the levelized cost of electricity (LCOE). This factor is the most commonly used parameter in the techno-economic analysis of different thermal power plants, which considers total investment costs C_{inv}, operation and maintenance costs $C_{O\&M}$, and total generated power during the whole year PG_{plant}. It can be calculated by the following equation [56]:

$$LCOE = \frac{crf.\ C_{inv} + C_{O\&M}}{PG_{plant}} \tag{33}$$

Where *crf* is the capital recovery factor and can be estimated as [56]:

$$crf = \frac{k_d.(k_d + 1)^N}{\left[(k_d + 1)^N - 1\right]} \tag{34}$$

where k_d is the annual discount rate and it is assumed to be 10.9% in the present work [67], and N is the depreciation operation time of the plant (25 years). At the same time, the total investment and O&M costs here are calculated based on data and correlations illustrated from the literature. These data and correlations are summarized in Tables 5 and 6 for the TPTPP, and the BBGPP, respectively.

3. Results and discussion

3.1. Validation

Regardless of the importance of model validation of different large-scale power plants, it is not easy to get actual data based on measurements to confirm the reliability of this model, since private companies erect most of these thermal power plants. Thus, the developed models in the present study have been validated with other numerical models from the literature. In the following two subsections, a short part has been reserved for the validation of the TPTPP and BBGPP.

3.1.1. TPTPP

The mathematical model incorporated in SAM for the energy analysis of the studied solar installation was validated by Price [68], by comparing the simulated data of a parabolic trough power plant using this model with real ones of SEGS VI plant. Furthermore, in a report published by the American National Renewable Energy Laboratory (NREL) [74], this model was established to simulate Andasol 1 parabolic trough power plant and showed a good agreement with this plant's actual data.

Table 4
Properties of organic fluids used in system design and simulation [24,25,64–66].

Fluid	T_{cri} [°C]	P_{cri} [kPa]	Δh_h [kJ/kg]	Vapor C_p[a] [J/kg.K]	ds/dT	*p-v-T* behavior	*ODP*	*GWP*
Group 1								
R143a	72.71	3761	226.6	1324.9	−1.75	Wet	0	328
R32	78.11	5782	381.8	1587.0	−5.67	Wet	0	677
R290	96.74	4251	425.6	2246.1	−3.29	Wet	0	3.3
Group 2								
R134a	101.06	4059	217.0	1280.6	−1.00	Isentropic	0	1300
Ammonia	132.25	11,333	1369.4	4448.0	−18.37	Wet	0.01	0
R142b	137.11	4055	223.2	1232.6	−0.73	Isentropic	0	2310
Group 3								
R245fa	154.01	3651	196.0	1301.8	0.30	Isentropic	0	1030
Pentane	196.55	3370	357.6	2367.7	1.18	Dry	0	4
Octane	296.17	2497	302.2	2648.8	3.05	Dry	–	–

[a] At boiling point.

Table 5
Costs data for the economic model of the TPTPP [56,59,67,68].

	Direct capital cost	
TPTPP	Site improvement	30.00 $/m^2
	Solar field	270.00 $/m^2
	HTF system	80.00 $/m^2
	TES system	80.00 $/kWh$_t$
	FBS system	60.00 $/kWe
	PB system	830.00 $/kWe
	Balance of the plant	105.00 $/kWe
	Contingency (of the direct capital cost)	7%
	Operation and maintenance costs	
	Fixed cost by capacity	65.00 $/kW-yr
	Variable cost by generation	3.00 $/MWh
	Fossil fuel cost	3.00 $/MMBtu

Table 6
Correlations to estimate the costs related to the BBGPP.

	Component	Cost function ($)
BBGPP	• Evaporator	$216.6 + 353.4A_{evap}$ [69,70]
	• Condenser	$338.6A_{cond}$ [69,70]
	• Turbine	$2237 \times (\dot{W}_{OT})^{0.41}$ [71]
	• Pump	$\left(\frac{\dot{W}_{OP}}{300}\right)^{0.25}$ [70]
	• Geothermal well	$16.5 \times H^{1.607}$ [72]
	• Operation and maintenance costs	1.5% of the installation cost [73]

3.1.2. BBGPP

In the present study, the mathematical model to simulate the bottoming BBGPP has been validated with another numerical model from the literature [46]. In turn, this model was established based on real data of an existing geothermal AFJET ORC power plant. The validation of the present thermodynamic analysis of the organic bottoming power block at design point with those reported by Ref. [46] has been reported in Table 7, where the variation of generated power with the variation of geothermal water inlet temperature to the evaporator for the two models is shown in Fig. 3. As it is observed in Table 7 and Fig. 4, the mathematical models to perform the energy analysis show excellent matching with that of [46], with slight differences of less than 0.37%, and 7.03% for the generated power and the energy efficiency, respectively. The source of these errors can be justified by the difference in the used thermophysical properties of the organic fluid between this study and the one presented by Ref. [46]. In addition, there is a lack of some data, such as the efficiencies of some components and pinch points. Nevertheless, the model shows a good correlation with that presented in Ref. [46], which confirms the viability of this model.

Table 7
Validation of the present thermodynamic analysis with Altun and Kilic model [46].

Parameter	Altun and Kilic model	Present model	e (%)
Generated power [MW]	2.7	2.69	0.37
Energy efficiency [%]	11.24	12.09	7.03

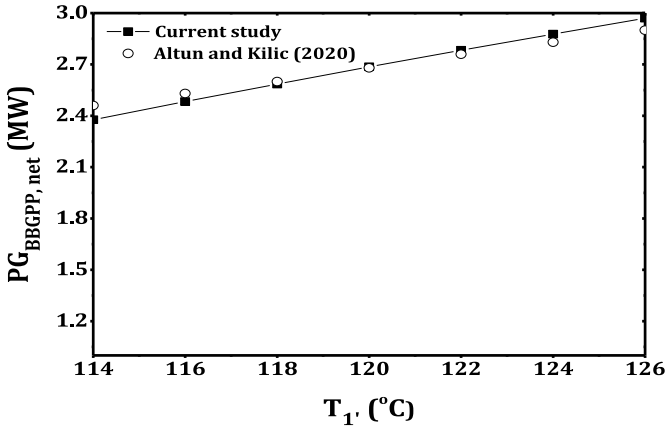

Fig. 4. Variation of $PG_{BBGPP,net}$ with the variation of geothermal inlet temperature in the two studies.

3.2. Performances of the new plant at nominal conditions

The equations presented in section 2.3, and previously mentioned inputs and assumptions in Tables 2 and 3, were applied to each component of the proposed design. So, each stream's thermodynamic properties, including the TPTPP and BBGPP (with R134a as working fluid), are calculated and given in Table 8. These properties, such as temperature, pressure, mass flow rate, enthalpy, and energy flow at each stage of the whole process, were estimated under nominal conditions, including DNI = 900 W/m^2, and $T_{1'} = 65$ °C. Also, the thermodynamic performances at these nominal conditions, including net power output and energy efficiency of the new configuration compared to stand-alone (parabolic trough power and binary geothermal power) plants, are presented in Table 9. As listed in this table, the total power output of the studied combined solar-geothermal plant is about 5.61 MW, where 3.62 MW is coming from the topping solar plant and the rest from the BBGPP (1.98 MW). Compared to the stand-alone plants, an improvement in power generation of the BBGPP (more than111%) has been recorded, although the same working conditions are applied on the three layouts to have a common ground for comparison. There is also a remarkable drop in the yield of the TPTPP (almost 23%). It can be explained by the rise of the condensing pressure of the topping plant to ensure the effectiveness of its cooling process, and such a procedure will reduce the generated power as it has been already discussed in section 2.2. On the

Table 8
Thermo-physical properties of the new plant at the nominal conditions.

No	Fluid	Fluid phase	T [°C]	P [kPa]	h [kJ/kg]	$\dot{m}$ [kg/s]	E [kW]
a	Molten salt	Liquid	290.0	1500	44.60	24.90	1110.54
b	Molten salt	Liquid	550.0	370	466.18	24.90	11607.882
c	Water/steam	Vapor	81.3	50	2645.2	3.57	9443.364
d	Water/steam	Liquid	81.3	50	340.5	3.57	1215.585
1	Geo water	Liquid	65.0	240	272.21	81	18,303
1′	Geo water	Liquid	86.96	240	346.31	81	29,509
2	Geo water	Liquid	35.0	240	146.76	81	11,887
3	R134a	Liquid	18.91	2503	225.96	86.79	19,611
4	R134a	Vapor	77.65	2503	429.00	86.79	37,232
5	R134a	Vapor	18.04	537.5	399.73	86.79	34,692
6	R134a	Liquid	18.04	537.5	224.69	86.79	19,500
7	Water	Liquid	25.0	220	104.95	600	62,968
8	Water	Liquid	31.6	220	130.27	600	78,159

Table 9
Yield analysis of the new considered plant compared to stand-alone configurations at the nominal conditions.

Parameter	Stand-alone PTTPP	Stand-alone BGPP	New plant
η_{TPTPP} [%]	–	–	12.65
η_{BBGPP} [%]	–	09.23	11.26
η_{Plant} [%]	16.40	–	14.45
Energy production [MW]	4.7	0.938	5.61
• Solar contribution [MW]	–	–	3.62
• Geothermal contribution [MW]	–	–	1.98

other side, this modification will increase the wasted heat recovered by the bottoming plant, thus, boosting the generated power of this last. Else, the efficiency of the TPTPP would have a decrease down to 12.65% (compared to 16.40% in stand-alone PTTPP), while that of the BBGPP would have an increase up to 11.26% (9.23% in stand-alone BGPP). However, the combined plant's global efficiency has been enhanced compared to the stand-alone solar plant (solar side of the Archimede plant) and this is justified by the recuperated waste heat by the BBGPP.

3.3. Comparative analysis of the studied plant with different fluids

For a better comparison of the studied configuration with different fluids circulating in the BBGPP, the effects of solar and geothermal resources on the performances of the proposed layouts (with nine different organic fluids) have been studied and presented in Figs. 5–8 in terms of energy efficiency and generated power of the BBGPP. Moreover, annual yield analyses of these nine layouts are shown in Table 10 and Fig. 9, and they are discussed to choose the best layout to be adopted in this new combined plant. As shown in Figs. 5–6, it is quite clear that there is a direct relationship between the generated power and energy efficiency of the BBGPP from a side, and solar resources represented by direct normal irradiance (DNI) from the other side. This enhancement is logical considering the augmentation in the wasted heat recuperated from the condenser of the topping solar plant, thus, the generated power by the bottoming cycle. The same note for the geothermal resources represented by the geothermal production temperature $T_{1'}$ is occurred, and it is always due to increases in energy received by the BBGPP. Going deep in the nine curves of each presented Figures (5-8), which match the nine layouts of the studied combined plant, it seems that four fluids (R143a, R32, R290, and ammonia) are more efficient compared to the others.

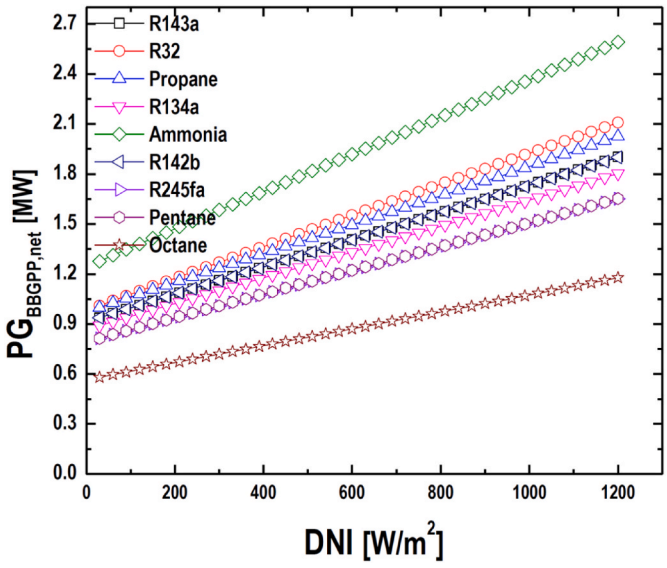

Fig. 5. Effect of DNI on the BBGPP generated power of the nine proposed layouts.

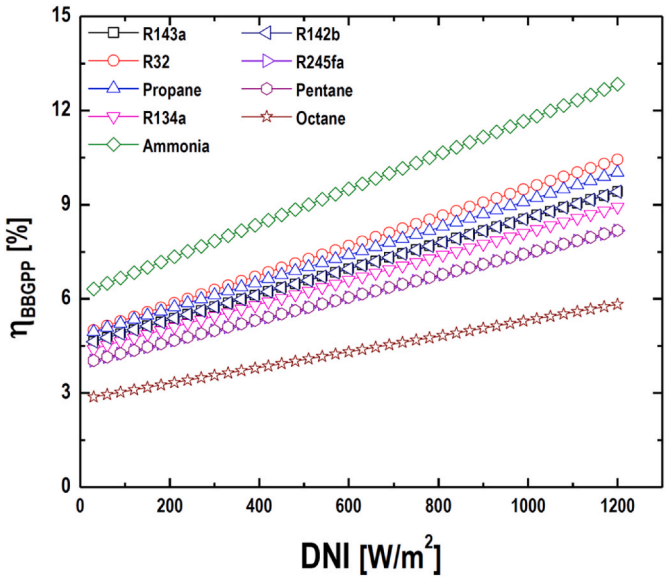

Fig. 6. Effect of DNI on the BBGPP energy efficiency of the nine proposed layouts.

These fluids belong to the two first groups (T_{cri} <100 °C, and 100 < T_{cri} <150 °C), while organic fluids classified in the third group (150 < T_{cri} < 300 °C) are the worst. Always and according to Table 4, the fluids with that performed well in the studied combined plant are those with wet behavior, which will facilitate the wasted heat recuperation by the bottoming cycle. For example, the studied plant with ammonia, which represents the most efficient layout (in term of yield), the energy efficiency as well as the energy production of the BBGPP vary from low values of 4.36% and 1.58 MW at a geothermal production temperature of 50 °C to the highest values of 14.20% and 5.18 MW at $T_{1'}$ = 120 °C respectively. Moving to R32 which is defined as the second-best candidate according to the obtained results, its layout shows the second-best performances as $\eta_{BBGPP} = 3.64 - 12.40\%$ and $PG_{BBGPP} = 1.32 - 4.51\ MW$ at geothermal production temperatures range from 50 °C to 120 °C respectively. Regarding the worst fluids, it seems that Octane and pentane are the atrocious choices from an energy performance point of

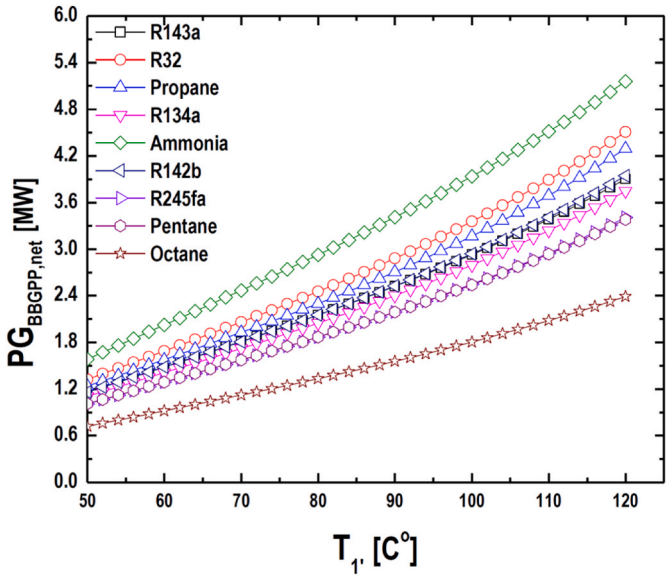

Fig. 7. Effect of geothermal production temperature on the BBGPP generated power of the nine proposed layouts.

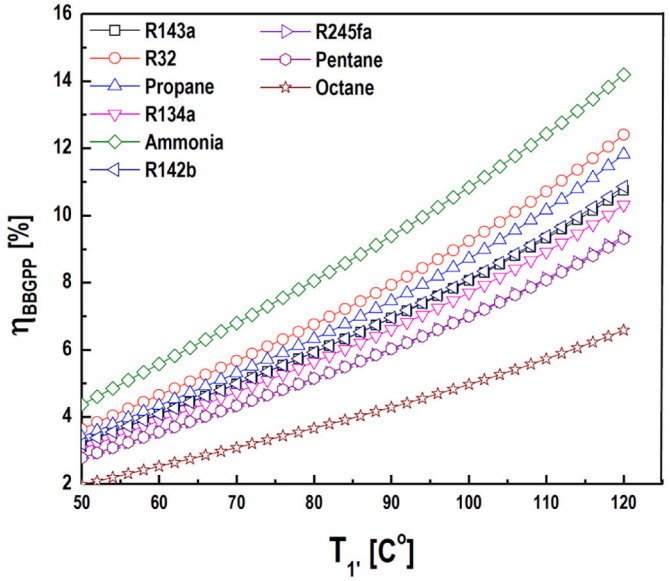

Fig. 8. Effect of geothermal production temperature on the BBGPP energy efficiency of the nine proposed layouts.

view.

In order to perform the annual simulations of the proposed combined plant, TMY data of El Oued (Algeria), including direct normal irradiance DNI, ambient temperature, and wind speed with 1-h interval data set, were generated using Meteonorm software [75]. The temperature of the geothermal production well was assumed to be fixed at the value of 65 °C. The same conclusion can be illustrated from annual results, where Fig. 9 shows the generated power of the new combined solar-geothermal power plant with the nine different layouts, including the stand-alone parabolic trough power plant (SAPTPP). At the same time, Table 10 depicts the annual comparative energy analysis of the configurations mentioned above. These simulations were obtained at the chosen site described in section 2.1. As presented and discussed in the previous paragraph, due to their wet behavior, the new studied plant with ammonia, R32, R290, and R143a, has the highest performances (14.64/13.20/12.70/12.32, and 22.20/20.02/19.25/18.67 GWhe) for global efficiency and annual power generation respectively. On the other hand, the new combined plant shows higher power generation and capacity factors compared to those of the SAPTPP no matter the adopted layout. For example, the studied combined plant with ammonia as the primary working fluid in the bottoming installation enhances the plant's dispatch capacity by 111.43 and 98% for annual power generation and capacity factor, respectively. However, there is a drop in solar contribution of the new plant compared to the conventional SAPTPP due to the rise of condensing pressure, which decreases the generated power as mentioned in section 3.2. Another critical point can be noted from Table 10, where the global efficiency of the whole combined plant has been decreased compared to the SAPTPP (from 16.71 to 14.64%). This drop can be explained by the decrease in solar-to-electricity efficiency of the topping cycle, and the increase in energy received by the geothermal side of the plant.

Moving to the thermo-economic dimension of the studied layouts, represented by two parameters; the total investment costs (Ctot), and the levelized cost of electricity (LCOE). As illustrated in Table 10, the investment costs of the hybrid plant increased compared to stand-alone plant, which is logical due to the inclusion of the investment costs of the

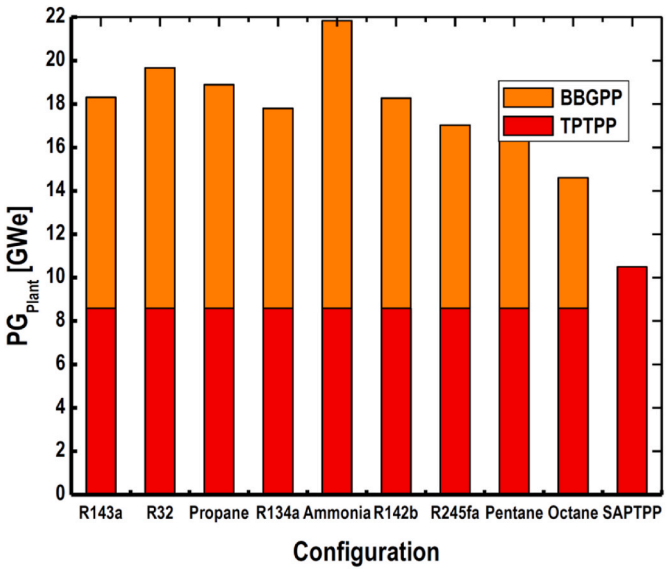

Fig. 9. Annual power generation of the nine proposed layouts.

Table 10
Comparison in annual performances of the new considered plant with the nine different organic fluids.

Parameter	R143a	R32	Propane	R134a	Ammonia	R142b	R245fa	Pentane	Octane	Stand-alone PTTPP
η_{BBGPP} [%]	10.98	12.50	11.63	10.41	14.97	10.94	9.53	9.54	6.80	–
$PG_{BBGPP,net}$ [GWhe]	9.72	11.08	10.31	9.22	13.26	9.69	8.44	8.45	6.02	–
η_{Plant} [%]	12.32	13.20	12.70	11.98	14.64	12.29	11.47	11.47	9.87	16.71
PG_{plant} [GWhe]	18.67	20.02	19.25	18.16	22.2	18.63	17.39	17.40	14.96	10.50
CF [%]	42.62	45.70	43.95	41.47	50.69	42.54	39.69	39.71	34.16	25.60
C_{tot} [M$]	28.38	29.16	28.68	27.77	29.60	26.85	24.71	24.03	26.19	22.807
LCOE [¢$/kWh]	11.88	11.39	11.65	11.96	10.42	11.27	11.1	10.81	13.69	16.98

BBGPP. Furthermore, the combined plant with pentane as the working fluid in the geothermal block has the lowest investment costs (24.03 M $), while the one working with ammonia has the highest (more than 29.60 M$). This difference can be explained by the increase in the surface areas of the heat exchangers, and the produced/used power by the turbine/pump of the BBGPP and its operating and maintenance costs. In another way, increasing the latent heats of the organic fluid will increase the surface areas of the heat exchangers to ensure the full heat exchange between the geothermal/cooling water and the ORC fluid. On the other hand, increasing the produced/used power by the turbine/pump will increase its costs. On the other hand, since the values of the LCOE depend totally on the investment costs and the annual power generation of the plant, as presented in the last row of Table 10, it varies from the lowest value of 10.42 ¢/kWh (ammonia configuration) to the highest value of 16.98 ¢/kWh (Stand-alone PTTPP).

4. Conclusion

In this paper, a design of a combined parabolic trough-geothermal thermal power plant has been proposed to enhance the dispatch capacity of this kind of thermal plants, and the effects of solar and geothermal resources on its yield have been analyzed. In this plant, the topping solar layout (TPTPP) is based on a conventional parabolic trough technology similar to that of solar side of Archimede plant, and integrated with thermal storage and fuel backup systems, while the bottoming binary geothermal (BBGPP) configuration is similar to AFJET geothermal power plant. Furthermore, nine organic fluids have been selected as candidates in the BBGPP, and their thermo-economic performances have been examined to select the best organic fluid. The following points have been concluded from this work:

- Under nominal conditions (DNI = 900 W/m^2, and $T_{1'}$ = 65 °C), the dispatch capacity of the proposed solar-geothermal plant (with R134a as working fluid in the bottoming plant) has been improved in comparison to the conventional solar side of Archimede plant (from 4.7 MW to 5.61 MW), which represents a rate of more than 19.36%. However, the global efficiency has been dropped from 16.40% for the old stand-alone PTPP to 14.45% for the new concept.
- Raising solar resources can enhance the performances of the BBGPP, as they raise the recovered wasted heat from the TPTPP, thus, boost the yield of the new hybrid plant. The same remark can be made for the geothermal resources.
- It seems that organic fluids with wet behavior show better performances compared to those with dry one. In this regard; ammonia, R32, R290, and R143a are more efficient compared to the others, where annual net outputs of 22.20, 20.02, 19.25, and 18.67 GWh_e have been produced respectively. The same point can be concluded for the global efficiency and the capacity factor, where ammonia has the highest performances with 14.64% and 50.69%, respectively.
- Based on thermo-economic criteria, it appears that the configuration based on ammonia is the best with the lowest LCOE with a value of 10.42 ¢/kWh.

This work presents a new path to raise the dispatch capacity and power generation of thermal power plants and decrease their economic risks, especially those based on renewable energies, either by hybridization or by waste heat recovery. These techniques can be explored in other technologies besides solar and geothermal, such as thermal plants working with coal, natural gas, and biomass. At the end, this study presents a pre-analysis of the new plant. Some points should be considered in future works, and the economic analysis should be further discussed to determine the feasibility of this design compared to the conventional one, and select the best layout to be adopted in such systems. The environmental criterion should also be considered in the selection process of the organic fluid circulating in the BBGPP. Accordingly, screening and investigating novel and environmentally-friendly refrigerants with low-GWP such as HFO; including R1234yf and R1233zd(E) are highly recommended for future works.

Credit author statement

T.E. Boukelia: Writing – original draft, Methodology, Data curation, Investigation, Formal analysis. O. Arslan: Supervising, Writing – review & editing. S. Djimli: Visualization. Y. Kabar: Supervising.

Declaration of competing interest

The authors declare that they have no known competing financial interests or personal relationships that could have appeared to influence the work reported in this paper.

Data availability

No data was used for the research described in the article.

Acknowledgement

This work was supported by The Scientific and Technological Research Council of Turkey (TUBITAK) under the grant of 2221-Fellowships for Visiting Scientists and Scientists on Sabbatical Leave with grant number of 1059B211800625.

References

[1] Ho CK, Iverson BD. Review of high-temperature central receiver designs for concentrating solar power. Renew Sustain Energy Rev 2014;29:835–46.
[2] Li K, Liu C, Jiang S, Chen Y. Review on hybrid geothermal and solar power systems. J Clean Prod 2019;27:119481.
[3] Lentz Á, Almanza R. Parabolic troughs to increase the geothermal wells flow enthalpy. Sol Energy 2006;80(10):1290–5.
[4] Lentz Á, Almanza R. Solar–geothermal hybrid system. Appl Therm Eng 2006;26 (14–15):1537–44.
[5] Astolfi M, Xodo L, Romano MC, Macchi E. Technical and economical analysis of a solar–geothermal hybrid plant based on an Organic Rankine Cycle. Geothermics 2011;40(1):58–68.
[6] Zhou C, Doroodchi E, Moghtaderi B. An in-depth assessment of hybrid solar–geothermal power generation. Energy Convers Manag 2013;74:88–101.
[7] Zhou C. Hybridisation of solar and geothermal energy in both subcritical and supercritical Organic Rankine Cycles. Energy Convers Manag 2014;81:72–82.
[8] Ghasemi H, Sheu E, Tizzanini A, Paci M, Mitsos A. Hybrid solar–geothermal power generation: optimal retrofitting. Appl Energy 2014;131:158–70.
[9] Ayub M, Mitsos A, Ghasemi H. Thermo-economic analysis of a hybrid solar-binary geothermal power plant. Energy 2015;87:326–35.
[10] Cardemil JM, Cortés F, Díaz A, Escobar R. Thermodynamic evaluation of solar-geothermal hybrid power plants in northern Chile. Energy Convers Manag 2016; 123:348–61.
[11] Bonyadi N, Johnson E, Baker D. Technoeconomic and exergy analysis of a solar geothermal hybrid electric power plant using a novel combined cycle. Energy Convers Manag 2018;156:542–54.
[12] Keshvarparast A, Ajarostaghi SS, Delavar MA. Thermodynamic analysis the performance of hybrid solar-geothermal power plant equipped with air-cooled condenser. Appl Therm Eng 2020;5:115160.
[13] Jiang PX, Zhang FZ, Xu RN. Thermodynamic analysis of a solar–enhanced geothermal hybrid power plant using CO2 as working fluid. Appl Therm Eng 2017; 116:463–72.
[14] Nazari N, Heidarnejad P, Porkhial S. Multi-objective optimization of a combined steam-organic Rankine cycle based on exergy and exergo-economic analysis for waste heat recovery application. Energy Convers Manag 2016;127:366–79.
[15] Heberle F, Hofer M, Ürlings N, Schröder H, Anderlohr T, Brüggemann D. Techno-economic analysis of a solar thermal retrofit for an air-cooled geothermal Organic Rankine Cycle power plant. Renew Energy 2017;113:494–502.
[16] McTigue JD, Castro J, Mungas G, Kramer N, King J, Turchi C, Zhu G. Hybridizing a geothermal power plant with concentrating solar power and thermal storage to increase power generation and dispatchability. Appl Energy 2018;228:1837–52.
[17] Acar MS, Arslan O. Energy and exergy analysis of solar energy-integrated, geothermal energy-powered Organic Rankine Cycle. J Therm Anal Calorim 2019; 137(2):659–66.
[18] Li T, Hu X, Wang J, Kong X, Liu J, Zhu J. Performance improvement of two-stage serial organic Rankine cycle (TSORC) driven by dual-level heat sources of geothermal energy coupled with solar energy. Geothermics 2018;76:261–70.
[19] Bassetti MC, Consoli D, Manente G, Lazzaretto A. Design and off-design models of a hybrid geothermal-solar power plant enhanced by a thermal storage. Renew Energy 2018;128:460–72.

[20] Habibi H, et al. Working fluid selection for regenerative supercritical Brayton cycle combined with bottoming ORC driven by molten salt solar power tower using energy–exergy analysis. Sustain Energy Technol Assessments 2020;39:100699.
[21] Maali R, Khir T. Performance analysis of different orc power plant configurations using solar and geothermal heat sources. Int J Green Energy 2020;17(6):349–62.
[22] Calise F, d'Accadia MD, Macaluso A, Piacentino A, Vanoli L. Exergetic and exergoeconomic analysis of a novel hybrid solar–geothermal polygeneration system producing energy and water. Energy Convers Manag 2016;115:200–20.
[23] Boukelia TE, Arslan O A, Bouraoui. Thermodynamic performance assessment of a new solar tower-geothermal combined power plant compared to the conventional solar tower power plant. Energy 2021:121109.
[24] Wang S, Liu C, Li Q, Liu L, Huo E, Zhang C. Selection principle of working fluid for organic Rankine cycle based on environmental benefits and economic performance. Appl Therm Eng 2020;178:115598.
[25] Zhang T, Liu L, Hao J, Zhu T, Cui G. Correlation analysis based multi-parameter optimization of the organic Rankine cycle for medium-and high-temperature waste heat recovery. Appl Therm Eng 2021;188:116626.
[26] Sachdeva J, Singh O. Comparative evaluation of solarized triple combined cycle for different ORC fluids. Renew Energy 2021;163:1333–42.
[27] Cataldo F, Mastrullo R, Mauro AW, Vanoli GP. Fluid selection of Organic Rankine Cycle for low-temperature waste heat recovery based on thermal optimization. Energy 2014;72:159–67.
[28] Tchanche BF, Papadakis G, Lambrinos G, Frangoudakis A. Fluid selection for a low-temperature solar organic Rankine cycle. Appl Therm Eng 2009;29(11–12): 2468–76.
[29] Drescher U, Brüggemann D. Fluid selection for the Organic Rankine Cycle (ORC) in biomass power and heat plants. Appl Therm Eng 2007;27(1):223–8.
[30] Hærvig J, Sørensen K, Condra TJ. Guidelines for optimal selection of working fluid for an organic Rankine cycle in relation to waste heat recovery. Energy 2016;96: 592–602.
[31] Wang ZQ, Zhou NJ, Guo J, Wang XY. Fluid selection and parametric optimization of organic Rankine cycle using low temperature waste heat. Energy 2012;40(1): 107–15.
[32] Saloux E, Sorin M, Nesreddine H, Teyssedou A. Reconstruction procedure of the thermodynamic cycle of organic Rankine cycles (ORC) and selection of the most appropriate working fluid. Appl Therm Eng 2018;129:628–35.
[33] Xu W, Deng S, Zhao L, Zhao D, Chen R. Identification of key affecting parameters of zeotropic working fluid on subcritical organic Rankine cycle according limiting thermodynamic cycle. Energy Convers Manag 2019;197:111884.
[34] Frutiger J, Andreasen J, Liu W, Spliethoff H, Haglind F, Abildskov J, Sin G. Working fluid selection for organic Rankine cycles–Impact of uncertainty of fluid properties. Energy 2016;109:987–97.
[35] Fan W, Han Z, Li P, Jia Y. Analysis of the thermodynamic performance of the organic Rankine cycle (ORC) based on the characteristic parameters of the working fluid and criterion for working fluid selection. Energy Convers Manag 2020;211: 112746.
[36] Pezzuolo A, Benato A, Stoppato A, Mirandola A. The ORC-PD: a versatile tool for fluid selection and Organic Rankine Cycle unit design. Energy 2016;102:605–20.
[37] Mavrou P, Papadopoulos AI, Seferlis P, Linke P, Voutetakis S. Selection of working fluid mixtures for flexible Organic Rankine Cycles under operating variability through a systematic nonlinear sensitivity analysis approach. Appl Therm Eng 2015;89:1054–67.
[38] Desai NB, Bandyopadhyay S. Thermo-economic analysis and selection of working fluid for solar organic Rankine cycle. Appl Therm Eng 2016;95:471–81.
[39] Xia XX, Wang ZQ, Hu YH, Zhou NJ. A novel comprehensive evaluation methodology of organic Rankine cycle for parameters design and working fluid selection. Appl Therm Eng 2018;143:283–92.
[40] Chen G, An Q, Wang Y, Zhao J, Chang N, Alvi J. Performance prediction and working fluids selection for organic Rankine cycle under reduced temperature. Appl Therm Eng 2019;153:95–103.
[41] Wang X, Levy EK, Pan C, Romero CE, Banerjee A, Rubio-Maya C, Pan L. Working fluid selection for organic Rankine cycle power generation using hot produced supercritical CO2 from a geothermal reservoir. Appl Therm Eng 2019;149: 1287–304.
[42] Yağlı H, Koç Y, Kalay H. Optimisation and exergy analysis of an organic Rankine cycle (ORC) used as a bottoming cycle in a cogeneration system producing steam and power. Sustain Energy Technol Assessments 2021;44:100985.
[43] Akbari H, Sorin M. Thermal design and selection of the optimal working fluid for organic Rankine cycles based on the equivalent temperature concept. Appl Therm Eng 2020;168:114860.
[44] Giostri A, et al. Comparison of different solar plants based on parabolic trough technology. Sol Energy 2012;86(5):1208–21.
[45] Boukelia TE, Ghellab A, Laouafi A, Bouraoui A, Kabar Y. Cooling performances time series of CSP plants: calculation and analysis using regression and ANN models. Renewable Energy; 2020.
[46] Altun AF, Kilic M. Thermodynamic performance evaluation of a geothermal ORC power plant. Renew Energy 2020;148:261–74.
[47] Mecibah MS, Boukelia TE, Tahtah R, Gairaa K. Introducing the best model for estimation the monthly mean daily global solar radiation on a horizontal surface (Case study: Algeria). Renew. Renew Sust Energ Rev 2014;36:194–202.
[48] Ouali S, Hadjiat MM, Ait-Ouali A, Salhi K, Malek A. Cartographie et caractérisation des ressources géothermiques de l'Algérie. Revue des Energies Renouvelables 2018;21(1):54–61.
[49] Boukelia TE, Mecibah MS. Estimation of direct solar irradiance intercepted by a solar concentrator in different modes of tracking (case study: Algeria). Int J Ambient Energy 2013;36(6):301–8.
[50] Georgios Rekkas Ventiris. Archimede concentrated solar power plant dynamic simulation: control systems, heat transfer fluids and thermal energy storage. Politecnico Di Milano: Master of Science Thesis; 2021.
[51] Zare V. A comparative exergoeconomic analysis of different ORC configurations for binary geothermal power plants. Energy Convers Manag 2015;105:127–38.
[52] Gholizadeh T, Vajdi M, Rostamzadeh H. A new trigeneration system for power, cooling, and freshwater production driven by a flash-binary geothermal heat source. Renew Energy 2020;148:31–43.
[53] Cengel YA, Boles MA, Kanoglu M. Thermodynamics: an engineering approach. fifth ed. New York: McGraw-hill; 2011.
[54] Zavoico AB. Solar power tower design basis document, sand2001-2100. Sandia National Laboratories 2001. https://prod.sandia.gov/techlib-noauth/access-control.cgi/2001/012100.pdf. [Accessed 8 April 2021]. Last accessed.
[55] Wagner W, Pruß A. The IAPWS formulation 1995 for the thermodynamic properties of ordinary water substance for general and scientific use. J Phys Chem Ref Data 2002;31(2):387–535.
[56] Wagner MJ, Gilman P. Technical manual for the SAM physical trough model (No. NREL/TP-5500-51825). National Renewable Energy Laboratory (NREL) 2001. USA, https://www.nrel.gov/docs/fy11osti/51825.pdf. [Accessed 8 April 2021]. Last accessed.
[57] Dudley VE, et al. Test results: SEGS LS-2 solar collector. SAND94-1884. Sandia National Laboratories 1994. http://www.nrel.gov/csp/troughnet/pdfs/segs_ls2_solar_collector.pdf. [Accessed 8 April 2021]. Last accessed.
[58] Forristall R. Heat transfer analysis and modeling of a parabolic trough solar receiver implemented in engineering equation solver. Technical Report NREL/TP-550-34169. National Renewable Energy Laboratory 2003. Golden, Colorado, USA, https://www.nrel.gov/docs/fy04osti/34169.pdf. [Accessed 8 April 2021]. Last accessed.
[59] Boukelia TE, Bouraoui A, Laouafi A, Djimli S, Kabar Y. 3E (Energy-Exergy-Economic) comparative study of integrating wet and dry cooling systems in solar tower power plants. Energy 2020;200:117567.
[60] Wagner M. Methodology for constructing reduced-order power block performance models for CSP applications: preprint (No. NREL/CP-5500-49370). National Renewable Energy Lab. (NREL) 2010. USA, https://www.nrel.gov/docs/fy11osti/49370.pdf. [Accessed 8 April 2021]. Last accessed.
[61] Ghasemi H, Paci M, Tizzanini A, Mitsos A. Modeling and optimization of a binary geothermal power plant. Energy 2013;50:412–28.
[62] Hu S, Li J, Yang F, Yang Z, Duan Y. Thermodynamic analysis of serial dual-pressure organic Rankine cycle under off-design conditions. Energy Convers Manag 2020; 213:112837.
[63] Refprop, Reference NIST. Fluid thermodynamic and transport properties. Reference database. USA: National Institute of Standards and Technology; 2010. Version 9.0.
[64] Myhre G, et al. Anthropogenic and natural radiative forcing. In: Climate change 2013: the physical science basis. Contribution of working group I to the fifth assessment report of the intergovernmental panel on climate change. Cambridge University Press; 2013. p. 659–740. https://doi.org/10.1017/CBO9781107415324.018.
[65] Global Warming Potentials of ODS Substitutes. Science - ozone layer protection. US EPA; 2007. Archived from the original on 2010-10-16. Retrieved 2010-12-16, http://www.epa.gov/Ozone/geninfo/gwps.html. Last accessed 08.04.2021.
[66] Daniel JS, et al. Halocarbon scenarios, ozone depletion potentials, and global warming potentials. Scientific assessment of ozone depletion; 2006.
[67] Boudaoud S, Khellaf A, Mohammedi K, Behar O. Thermal performance prediction and sensitivity analysis for future deployment of molten salt cavity receiver solar power plants in Algeria. Energy Convers Manag 2015;89:655–64.
[68] NREL. System Advisor model (SAM) case study: Andasol-1. https://sam.nrel.gov/images/web_page_files/sam_case_csp_physical_trough_andasol-1_2013-1-15.pdf. Last accessed 08.04.2021.
[69] Quoilin S, Declaye S, Tchanche BF, Lemort V. Thermo-economic optimization of waste heat recovery Organic Rankine Cycles. Appl Therm Eng 2011;31(14–15): 2885–93.
[70] Lecompte S, Huisseune H, Van den Broek M, De Schampheleire S, De Paepe M. Part load based thermo-economic optimization of the Organic Rankine Cycle (ORC) applied to a combined heat and power (CHP) system. Appl Energy 2013;111: 871–81.
[71] Alshammari F, Karvountzis-Kontakiotis A, Pesyridis A, Usman M. Expander technologies for automotive engine organic Rankine cycle applications. Energies 2018;11(7):1905.
[72] Ahmadi A, Assad MEH, Jamali DH, Kumar R, Li ZX, Salameh T, Al-Shabi M, and Ehyaei MA. Applications of geothermal organic Rankine Cycle for electricity production. J Clean Prod 2020; 274 : 122950.
[73] Hu S, Yang Z, Li J, Duan Y. Thermo-economic optimization of the hybrid geothermal-solar power system: a data-driven method based on lifetime off-design operation. Energy Convers Manag 2021;229:113738.
[74] Price H. A parabolic trough solar power plant simulation model. ASME. Hawaii, USA: International Solar Energy Conference; 2003. 665-673.
[75] Meteonorm. World wide irradiation data. https://meteonorm.com/en/Last. [Accessed 10 November 2021]. accessed.